The Astrophysical Journal, 612:496–510, 2004 September 1

CONSTRAINING THE LIFETIME OF CIRCUMSTELLAR DISKS IN THE TERRESTRIAL PLANET ZONE: A MID-INFRARED SURVEY OF THE 30 Myr OLD TUCANA-HOROLOGIUM ASSOCIATION

Eric E. Mamajek, Michael R. Meyer, Philip M. Hinz, and William F. Hoffmann
Steward Observatory, Department of Astronomy, University of Arizona, 933 North Cherry Avenue, Tucson, AZ 85721; eem@as.arizona.edu

Martin Cohen
Radio Astronomy Laboratory, 601 Campbell Hall, University of California, Berkeley, CA 94720

and

Joseph L. Hora
Harvard-Smithsonian Center for Astrophysics, 60 Garden Street, MS-65, Cambridge, MA 02138
Received 2004 March 16; accepted 2004 May 13

ABSTRACT

We have conducted an *N*-band survey of 14 young stars in the ~30 Myr old Tucana-Horologium association to search for evidence of warm, circumstellar dust disks. Using the MIRAC-BLINC camera on the Magellan I (Baade) 6.5 m telescope, we find that none of the stars have a statistically significant *N*-band excess compared to the predicted stellar photospheric flux. Using three different sets of assumptions, this null result rules out the existence of the following around these post–T Tauri stars: (1) optically thick disks with inner hole radii of $\lesssim$0.1 AU, (2) optically thin disks with masses of less than $10^{-6}\,M_{\oplus}$ (in ~1 μm sized grains) within $\lesssim$10 AU of these stars, and (3) scaled-up analogs of the solar system zodiacal dust cloud with more than 4000 times the emitting area. Our survey was sensitive to dust disks in the terrestrial planet zone with fractional luminosity of $\log(L_{\rm dust}/L_*) \sim 10^{-2.9}$, yet none were found. Combined with results from previous surveys, these data suggest that circumstellar dust disks become so optically thin as to be undetectable at *N* band before age ~20 Myr. We also present *N*-band photometry for several members of other young associations and a subsample of targets that will be observed with the *Spitzer Space Telescope* by the Formation and Evolution of Planetary Systems Legacy Science Program. Finally, we present an absolute calibration of MIRAC-BLINC for four filters (*L*, *N*, 11.6, and Q_s) on the Cohen-Walker-Witteborn system.

Subject headings: circumstellar matter — infrared: stars — open clusters and associations: individual (Horologium, Tucana) — planetary systems: formation — planetary systems: protoplanetary disks

1. INTRODUCTION

Circumstellar disks appear to be a nearly ubiquitous by-product of the star formation process. Most low-mass stars in the youngest star formation regions (e.g., the ~1 Myr old Orion Nebula cluster) have spectroscopic or photometric evidence of a circumstellar disk (Hillenbrand et al. 1998). The masses of circumstellar disks found around some T Tauri stars are similar to that of the minimum mass solar nebula (Beckwith et al. 1990). Their physical sizes are similar to that of our own solar system (tens to hundreds of AU; McCaughrean & O'Dell 1996). Considering their masses, dimensions, and appearance at the very earliest stages of stellar evolution, these disks are considered "protoplanetary." Radial velocity surveys of nearby solar-type stars indicate that at least ~5% have at least one Jupiter mass planet orbiting within a few AU (Marcy & Butler 2000), indicating that the formation of gas giant planets is one likely outcome of circumstellar disk evolution.

The incidence of inner protoplanetary accretion disks diminishes with age, being very common at ages of less than 1 Myr and very rare at more than 10 Myr. The fraction of low-mass stars with disks inferred by IR excess (in the *L* band; 3.5 μm) diminishes with age, with half losing their inner disks ($\lesssim$0.1 AU) by age ~3 Myr (e.g., Haisch et al. 2001a). Using population statistics of pre–main-sequence stars in the Taurus molecular clouds, multiple studies have demonstrated that the transition time for disks inside of ~1 AU to go from optically thick to optically thin is $\sim 10^5$ yr (Skrutskie et al. 1990; Wolk & Walter 1996). While some studies argue that accretion terminates by age ~6 Myr (Haisch et al. 2001a), recent studies suggest that it may continue at lower accretion rates around some stars until at least age ~10 Myr (Muzerolle et al. 2000; Mamajek et al. 2002; Lawson et al. 2002, 2004). There are preliminary indications that disks may persist longer for stars in associations that lack massive OB stars and for the lowest mass stars (e.g., Lyo et al. 2003; Haisch et al. 2001b). Although understanding the evolution of accretion disks has improved, the evolution of dust in the terrestrial planet zone is still largely unexplored.

Although the phenomenon of optically thick accretion disks appears to be isolated to the first ~few Myr of a star's life, numerous examples of older stars with optically thin dust disks have been found over the past two decades, primarily using space-based IR telescopes, e.g., the *Infrared Astronomical Satellite* (*IRAS*) and the *Infrared Space Observatory* (*ISO*) (Backman & Paresce 1993; Lagrange et al. 2000). Optically thin disks have been found around stars over a wide range of ages and masses, but those with the highest fractional luminosity ($f_d = L_{\rm disk}/L_*$) are mostly confined to those younger than a few $\times$ 100 Myr in age (Habing et al. 2001; Spangler et al. 2001). These dusty "debris" disks are inferred to be created by the collisions of larger bodies, rather than primordial interstellar medium (ISM) dust (Harper et al. 1984; Backman & Paresce 1993). For micron-sized dust grains orbiting between

TABLE 1
MIRAC Observations of Tuc-Hor Members

UT Date (1)	Star Name (2)	Band (3)	On-Source Time (s) (4)	Flux Standards (5)
2001 Aug 8	HIP 105388	*N*	300	ι Cet, α CMa
	HIP 105404	*N*	600	ι Cet, α CMa
	HIP 107947	*N*	600	ι Cet, α CMa
	HIP 108195	*N*	360	ι Cet, α CMa
	HIP 116748 AB	*N*	600	ι Cet, α CMa
	HIP 1481	*N*	480	ι Cet, α CMa
	HIP 1910	*N*	840	ι Cet, α CMa
	HIP 2729	*N*	840	ι Cet, α CMa
2001 Aug 9	HIP 490	*N*	420	ι Cet, η Sgr, α CMa
	HIP 6485	*N*	600	ι Cet, η Sgr, α CMa
	HIP 6856	*N*	660	ι Cet, η Sgr, α CMa
	HIP 9892	*N*	840	ι Cet, η Sgr, α CMa
	ERX 37 N	*N*	1020	ι Cet, η Sgr, α CMa
2001 Aug 10	HIP 9685	*N*	690	α Cen, ι Cet, η Sgr
2002 Aug 21	HIP 1910	*N*	180	γ Cru, η Sgr, ι Cet

$\sim$0.1 and 10 AU, the timescale for Poynting-Robertson (P-R) drag to pull the grains into the star ($\sim 10^1$–10^5 yr) is short compared to typical stellar ages ($\sim 10^7$–10^{10} yr), implying either that the observed phenomena are short lived or that grains must be replenished through collisions of larger bodies. There is preliminary evidence for a monotonic decrease in dust disk optical depth with age (Spangler et al. 2001) or possibly a more precipitous drop in optical depth after age $\sim$400 Myr (Habing et al. 2001). Most of the known debris disks have been identified by excess far-IR emission above that of the stellar photosphere (e.g., Silverstone 2000), with characteristic dust temperatures of $\sim$30–100 K. Despite efforts to find warm ($T \sim 200-300$ K) dust disks around field stars, precious few examples with detectable 10–12 μm excesses are known (Aumann & Probst 1991).

Observational constraints on the evolution of circumstellar dust in the terrestrial planet zone are currently scarce. Planned observations with the recently launched *Spitzer Space Telescope* by the Formation and Evolution of Planetary Systems (FEPS) Legacy Science Program,[1] among others, will remedy this situation. FEPS plans to systematically trace the evolution of circumstellar gas and dust around Sun-like stars between the epoch of optically thick accretion disks (ages $\sim$ a few Myr) to the epoch of mature planetary systems (ages $\sim$ a few Gyr; Meyer et al. 2002, 2004).

Although *Spitzer* promises to provide a leap in our understanding of the circumstellar environs of stars, we can address a basic question about disk evolution using currently available ground-based facilities. *How much dust remains within a few AU of young stars during the epoch of terrestrial planet formation?* We address this question through a mid-IR survey of a sample of young, low-mass stars with ages of $\sim$30 Myr: the Tuc-Hor association.

Dynamical simulations suggest that, given the surface mass density of the minimum-mass solar nebula, runaway growth can take place and form Moon-sized planetary "embryos" within $\sim 10^5$ yr (Wetherill & Stewart 1993). When the largest embryos reach radii of $\sim$1000 km, gravitational interactions increase the eccentricities and collision velocities of smaller planetesimals, causing more dust-producing collisions (Kenyon & Bromley 2004). Over the next $\sim 10^7$–10^8 yr, the growth of the largest embryos is dominated by giant impacts, which consolidate the embryos into a small number of terrestrial planets (Agnor et al. 1999; Chambers 2001). During this epoch in our own solar system, the proto-Earth is hypothesized to have been impacted by a Mars-sized planetesimal, which formed the Earth-Moon system (Hartmann & Davis 1975; Stevenson 1987). Chronometry studies using radioactive parent-daughter systems (such as ^{182}Hf-^{182}W) suggest that the Earth-Moon impact occurred 25–35 Myr after the formation of the solar system (Kleine et al. 2002, 2003). We know that around at least one star (our Sun), terrestrial planets were forming at age $\sim$30 Myr.

In § 2 we describe the sample, our mid-IR observations, and data reduction. Section 3 presents the results of our photometry. We present three simple circumstellar disk models in § 4 and calculate upper limits to the amount of dust orbiting within $\lesssim$10 AU of the stars observed. In § 5 we discuss our results in light of previous observational and theoretical efforts in order to better understand disk evolution around young stars. In Appendices A and B we present information related to the photometric calibration of the MIRAC-BLINC system, as well as details regarding stars for which mid-IR excesses were detected.

2. OBSERVATIONS

2.1. *The Sample*

Our mid-IR survey contains 14 low-mass stars that we argue are probable members of the $\sim$30 Myr old Tuc-Hor association. The observations of the Tuc-Hor stars are presented in Table 1. Observations of some Tuc-Hor candidates that we reject as members and other young stars (some of which are FEPS *Spitzer* Legacy Science targets) are included in Table 2. Here we discuss some technical aspects of the Tuc-Hor sample.

The Tucana and Horologium associations are young stellar moving groups that were identified nearly contemporaneously by Zuckerman & Webb (2000, hereafter ZW00) and Torres et al. (2000, hereafter TDQ00). Zuckerman et al. (2001b, hereafter ZSW01) present an updated membership list and photometry and suggest that the similar ages, kinematics, and

[1] See http://feps.as.arizona.edu.

TABLE 2
MIRAC Observations of Other Stars

UT Date (1)	Star Name (2)	Band (3)	On-Source Time (s) (4)	Flux Standards (5)
2001 Aug 6	GJ 799 AB	11.6	135	ι Cet
	GJ 803	11.6	165	ι Cet
	HIP 108195	11.6	60	ι Cet
2001 Aug 7	HIP 99273	11.6	255	α Car, α PsA, γ Cru
2001 Aug 8	HD 143006	*N*	60	ι Cet, α CMa
	HD 143006	11.6	120	γ Cru
	[PZ99] J161318.6−221248	*N*	600	ι Cet, α CMa
	HD 181327	*N*	240	ι Cet, α CMa
	HR 7329	*N*	60	ι Cet, α CMa
2001 Aug 9	RX J1853.1−3609	*N*	960	ι Cet, η Sgr, α CMa
	RX J1917.4−3756	*N*	660	ι Cet, η Sgr, α CMa
2001 Aug 10	HIP 63797	*N*	300	α Cen, ι Cet, η Sgr
	[PZ99] J161411.0−230536	*N*	360	α Cen, ι Cet, η Sgr
	ScoPMS 214	*N*	450	α Cen, ι Cet, η Sgr
	ScoPMS 5	*N*	450	α Cen, ι Cet, η Sgr
	HIP 95149	*N*	360	α Cen, ι Cet, η Sgr
	HIP 113579	*N*	510	α Cen, ι Cet, η Sgr
	HIP 1134	*N*	480	α Cen, ι Cet, η Sgr
2002 Aug 21	HIP 93815	*N*	180	γ Cru, η Sgr, ι Cet
	HIP 99803A	*N*	690	γ Cru, η Sgr, ι Cet
	HIP 99803B	*N*	165	γ Cru, η Sgr, ι Cet
	HIP 105441	*N*	360	γ Cru, η Sgr, ι Cet
	HIP 107649	*N*	240	γ Cru, η Sgr, ι Cet
	PPM 366328	*N*	180	γ Cru, η Sgr, ι Cet
	HIP 108809	*N*	360	γ Cru, η Sgr, ι Cet
	HIP 108422	*N*	300	γ Cru, η Sgr, ι Cet
	GJ 879	*N*	240	γ Cru, η Sgr, ι Cet

positions of the Tucana and Horologium associations allow us to consider them a single group (''Tuc-Hor''). We adopt $\sim$30 Myr as a reasonable age estimate for Tuc-Hor based on recent values in the literature (see Table 3).

The published membership lists for Tuc-Hor appear to be somewhat subjective and contain some stars that are unlikely to be members. In order to include stars that are plausibly members of Tuc-Hor as part of our study, we used kinematics as the primary membership criterion (in addition to the other criteria used in previous studies). For the combined Tuc-Hor membership lists of TDQ00, ZW00, ZSW01, we calculate membership probabilities using the equations of de Bruijne (1999), the heliocentric space motion of the Tucana nucleus from ZW00, and the best long-baseline proper motions available at present (preferably Tycho-2 or UCAC2; Høg et al. 2000; Zacharias et al. 2004). We reserve rigorous discussion of membership and kinematics for a separate future study. For this study, we retain only those stars whose membership we could not reject based on proper motion data. We find that $\sim$30% of the stars proposed as members of Tuc-Hor have proper motions inconsistent with the motion of the assumed Tucana ''nucleus'' (centered on the β Tuc minicluster; using space motion vector given by ZW00). The published membership lists appear to contain several field stars, a handful of which we observed with MIRAC (Table 2) before appreciating that they were probable nonmembers. Care should be used by investigators employing samples of recently discovered, diffuse stellar associations (e.g., Tuc-Hor) for the study of age-dependent stellar phenomena.

We include in our Tuc-Hor sample the active dwarf HD 105 (=HIP 490). HD 105 is in the same region of sky ($\alpha = 00^{\rm h}05^{\rm m}$, $\delta = -41^\circ45'$ [International Celestial Reference System]) as the other proposed Tuc-Hor stars and has a *Hipparcos* distance of $d = 40$ pc. For our calculations we adopt the long-baseline Tycho-2 proper motion (Høg et al. 2000) and the Tuc-Hor space motion vector from ZW00. In subjecting HD 105 to the

TABLE 3
Age Estimates for Tucana-Horologium Association

Reference (1)	Group (2)	Age (Myr) (3)	Method (4)	Notes (5)
ZW00	Tuc	40	Hα emission	Comparing Hα emission of three stars to α Per members
TDQ00	Hor	30	Theoretical isochrones	Siess et al. (1997) tracks
Torres et al. (2001)	Tuc-Hor	20	Velocity dispersion	''GAYA'' = Tuc-Hor
Stelzer & Neuhäuser (2001)	Tuc	10–30	X-ray emission	Member $L_{\rm X}$ values similar to TWA, Tau-Aur, and IC 2602
ZSW01	Tuc	10–40	Theoretical isochrones	K and M stars; Siess et al. (2000) tracks

same kinematic tests as the other Tuc-Hor candidates, we are unable to reject its membership. The calculated cluster parallax (25.3 mas) and predicted radial velocity (0 km s^{-1}) agree very well with the observed trigonometric parallax (24.9 ± 0.9 mas; ESA 1997) and measured radial velocity ($+1.7 \pm 2.5$ km s^{-1}; Wichmann et al. 2003). The equivalent width of the Li I λ6707 line (165 mÅ; Cutispoto et al. 2002) is similar to that for early G-type members of the ~50 Myr old IC 2602 and IC 2391 clusters (Randich et al. 2001) and stronger than that found in ~120 Myr old Pleiades stars (Soderblom et al. 1993). Finally, the X-ray luminosity of HD 105 [$\log(L_X) = 29.4$ ergs s^{-1}; Cutispoto et al. 2002] is similar to what is expected for early-G stars with ages of 10–100 Myr (Briceño et al. 1997). Therefore, we conclude that HD 105 is a likely member of the Tuc-Hor association.

2.2. *Data Acquisition*

Mid-IR images of the Tuc-Hor members and other young stars were obtained during the nights of 2001 August 6–10 and 2002 August 22 (UT) with the MIRAC-BLINC instrument on the Magellan I (Baade) 6.5 m alt-az telescope at Las Campanas Observatory, Chile. The Mid-Infrared Array Camera (MIRAC3) contains a Rockwell HF16 128×128 hybrid BIB Si:As array and was built at the Steward Observatory, University of Arizona, and the Harvard-Smithsonian Center for Astrophysics (Hoffmann et al. 1998). The Bracewell Infrared Nulling Cryostat (BLINC) is a nulling interferometer mated to MIRAC3 (Hinz et al. 2000). In our observing mode, however, BLINC is used as a reimaging system, reducing the f/11 beam from the Magellan tertiary mirror to a f/20 beam required for the MIRAC3 instrument. The pixel scale is 0.″123 $pixel^{-1}$, resulting in a field of view of 15.″7.

Our intent was to survey for circumstellar dust surrounding our target stars in the terrestrial planet zone (~0.3–3 AU), with characteristic temperatures of ~300 K and a corresponding Wien emission peak at ~10 μm. Observations were obtained with either the wideband *N* filter ($\lambda_{iso} = 10.34$ μm for an A0 star, where λ_{iso} is the isophotal wavelength; e.g., Golay 1974) or the narrowband "11.6" filter ($\lambda_{iso} = 11.57$ μm for an A0 star) in standard chop-nod mode (four-position beam-switching; see Appendix 1 of Hoffmann & Hora 1999). The nod and chop separations were 8″, and the chop (frequency of 3–10 Hz) was in a direction perpendicular to the nod vector. The chop-nod imaging technique produces two positive and two negative images of the star in a square configuration on the detector. The nod separation was chosen so that all four images of the star appear on the detector with sufficient room for determination of the background flux in annuli surrounding each star image. We found that using chop frequencies of between 3 and 10 Hz mitigated the effects of poorly subtracted sky background (background noise increases as chop frequency decreases) while maintaining observing efficiency (increasing the chop frequency adds overhead time, with minimal improvement in background subtraction). Chopping was done with an internal pupil plane beam-switching mirror within BLINC. The frame time (on-chip integration time) was either 10 ms (*N* band) or 40 ms (11.6 band), and these frames were coadded in 15–30 s long integrations per nod beam. We found that derotating the MIRAC-BLINC instrument (i.e., freezing the cardinal sky directions on the detector) in the Nasmyth port during observations resulted in poorer background subtraction compared to turning the derotation off. Hence, for the majority of observations taken during these nights, the instrument derotation was turned off. The ability to guide the telescope while derotating the instrument was not available during our observing runs. Hence the telescope was not guiding during most of our observations. This had negligible impact on the achieved image quality but limited our ability to reliably co-add data for faint sources.

2.3. *Reduction*

The MIRAC images were reduced using the custom program *mrc2fts* (Hora 1991) and IRAF[2] routines. Flat fields were constructed from images of high (dome) and low (sky) emissivity surfaces. A median sky frame was produced and subtracted from the individual ($N \simeq 10$) dome frames. The results were then median combined to produce the final flat field. The pixel-to-pixel variation in sensitivity (~2% rms) of the MIRAC detector is small enough that flat-fielding had negligible effect on our derived photometry.

Aperture photometry was derived using the IRAF *phot* package. We used aperture radii of either 0.″62 (5 pixels) or 1.″23 (10 pixels), depending on which flux had the higher signal-to-noise ratio (S/N) after the photometric errors were fully propagated (dominated by sky noise for large aperture or uncertainty in aperture correction for smaller apertures). The photometry derived with aperture radii of 5 and 10 pixels was consistent within the errors for all of the stars observed. The background level was determined by measuring the mean sky value per pixel in an annulus centered on the star with inner radius 1.″85 (15 pixels) and outer radius 3.″08 (25 pixels) for subtraction. The background annulus radii were chosen so as to sample a negligible contribution of the star's point-spread function (PSF), but to avoid the PSFs from the other images of the same star. For the faintest sources, an aperture radius of 5 pixels was usually used, in which case an aperture correction was applied to place all photometry on the 10 pixel system. The aperture corrections were determined nightly using standard stars, and the typical correction to the 5 pixel aperture radius photometry was -0.32 ± 0.05 mag. Photometric solutions (zero points and air-mass corrections) were determined for every night of observations. The typical air-mass corrections at *N* band were 0.1–0.2 mag per air mass. The conversion between fluxes (in mJy) and magnitudes is simply $\mathrm{mag}_\lambda(\mathrm{star}) = -2.5 \log[f_\lambda(\mathrm{star})/f_\lambda(0)]$, where $f_\lambda(\mathrm{star})$ is the star's flux at wavelength λ and $f_\lambda(0)$ is the flux of a zero-magnitude star (see Appendix A). The sensitivity was such that we could detect a star with magnitude 7.5 in *N* band at $S/N \simeq 5$ with 600 s of on-source integration time.

We observed standard stars taken from the MIRAC manual (Hoffmann & Hora 1999), the list of ESO IR standards (van der Bliek et al. 1996), and the list of Cohen et al. (1999). M. C. calculated an independent calibration of the MIRAC photometric system using an approach identical to that described in Cohen et al. (2003a). Discussion on the input data for the absolute photometric calibration, the zero-magnitude attributes of the MIRAC filter systems, and standard-star fluxes are given in Appendix A. The absolute accuracy of the standard-star fluxes among the four filters ranges from 1.7% to 4.5%.

3. RESULTS

N-band photometry for young stars in Tuc-Hor is presented in Table 4, while photometry for stars in other regions (most

[2] IRAF is distributed by the National Optical Astronomy Observatory, which is operated by the Association of Universities for Research in Astronomy, Inc., under cooperative agreement with the National Science Foundation. See http://iraf.noao.edu.

TABLE 4
N-Band Photometry of Tuc-Hor Members

Hipparcos Name (1)	Other Name (2)	Spectral Type (3)	K_s (mag) (4)	Predicted F_ν (mJy) (5)	Measured F_ν (mJy) (6)	$E(N)$ (mJy) (7)	Deviation (σ) (8)
HIP 490.....	HD 105	G0	6.12 ± 0.02	139	138 ± 8	−1 ± 8	−0.2
HIP 1481.....	HD 1466	F8	6.15 ± 0.02	135	151 ± 20	+16 ± 20	+0.8
HIP 1910.....	BPM 1699	M0	7.49 ± 0.02	51	49 ± 7	−2 ± 7	−0.3
HIP 2729.....	HD 3221	K4	6.53 ± 0.02	111	102 ± 5	−9 ± 5	−1.7
HIP 6485.....	HD 8558	G6	6.85 ± 0.03	71	82 ± 4	+11 ± 4	+2.4
HIP 6856.....	HD 9054	K2	6.83 ± 0.02	72	85 ± 4	+13 ± 4	+3.0
HIP 9685.....	HD 12894	F4	5.45 ± 0.02	258	207 ± 17	−51 ± 18	−2.9
HIP 9892.....	HD 13183	G5	6.89 ± 0.02	68	67 ± 6	−1 ± 6	−0.2
ERX 37 N.....	AF Hor	M3	7.64 ± 0.03	42	46 ± 3	+4 ± 3	+1.3
HIP 105388.....	HD 202917	G5	6.91 ± 0.02	67	65 ± 9	−2 ± 9	−0.3
HIP 105404.....	HD 202947	K0	6.57 ± 0.02	92	74 ± 9	−18 ± 9	−1.9
HIP 107947.....	HD 207575	F6	6.03 ± 0.02	151	155 ± 12	+4 ± 12	+0.3
HIP 108195.....	HD 207964	F3	4.91 ± 0.02	424	394 ± 20[a]	−30 ± 21	−1.4
HIP 116748A.....	HD 222259A	G6	6.68 ± 0.03	83	75 ± 12	−8 ± 12	−0.7
HIP 116748B.....	HD 222259B	K	7.03 ± 0.06	60	53 ± 14	−7 ± 14	−0.5

Notes.—Col. (1): *Hipparcos* name. Col. (2): Other name. Col. (3): Spectral type from either ZW00, TDQ00, or ZSW01. Col. (4): K_s magnitude from 2MASS (Cutri et al. 2003). Col. (5): Measured MIRAC *N*-band flux. Col. (6): Predicted photospheric flux. Col. (7): Flux excess and uncertainty. Col. (8): Residual deviation = $E(N)/\sigma[E(N)]$. ERX 37 N is given in SIMBAD as [TDQ2000] ERX 37 N. Predicted *N*-band photospheric fluxes use or assume 2MASS K_s magnitudes, $A_V = 0$, dwarf color relations from § 3, and zero-magnitude flux of 37.25 Jy for *N*-band.

[a] HIP 108195 was also imaged at 11.6 μm with a flux of 284 ± 40 mJy.

belonging to young, nearby associations) is presented in Table 5. Near-infrared (JHK_s) photometry from the 2MASS catalog (Cutri et al. 2003) was used to help predict the brightness of the stellar photospheres at 10 μm. For the range of spectral types investigated, models predict that $[11.6] - N \simeq 0.00$ within our photometric errors (typically ∼0.05–0.10 mag); hence we plot $K_s - N$ and $K_s - [11.6]$ on the same color-color plot and generically refer to these colors as "$K_s - N$" throughout. A color-color plot of the Tuc-Hor stars is illustrated in Figure 1.

Figure 1 indicates that $K_s - N$ colors are fairly uniform for stars with $J - K_s < 0.7$, i.e., for FGK stars. We decided to analyze the M stars separately from the FGK stars. We surmise that much of the structure in the published color-color relations for dwarfs is probably due to statistical fluctuations (e.g., Cohen et al. 1987; Waters et al. 1987; Mathioudakis & Doyle 1993; Kenyon & Hartmann 1995). After examining our data and those from previous studies of large dwarf samples, we decided to assume a constant $K_s - N$ color for the photospheres of FGK stars. In calculating a mean intrinsic $K_s - N$ color, we include the FGK stars in Tables 4 and 5 but exclude the FGK stars HD 143006 and [PZ99] J161411 (both with $K_s - N \simeq 2$) and HIP 95270 and HIP 99273 (known to have far-IR excesses that may contaminate *N*-band flux; e.g., Zuckerman & Song 2004). The median, unweighted-mean, and weighted-mean $K_s - N$ colors for the FGK stars are all similar (0.05, 0.04 ± 0.02, and 0.07 ± 0.02, respectively). These estimates agree well with the mean FGK dwarf color found by Fajardo-Acosta et al. (2000; $K_s - [12] \simeq +0.04$ implies $K_s - N \simeq +0.05$) and are close to the value for AFGK-type dwarfs found by Aumann & Probst (1991; $K_{CIT} - [12] = +0.02$, implying $K_s - N = +0.01$).[3] Within the uncertainties, *our measured mean $K_s - N$ color for FGK dwarfs is consistent with previous determinations. The mean colors for the young stars in our observing program do not appear to be biased toward red $K_s - N$ colors because of the presence of circumstellar material.* We adopt $(K_s - N)_{phot} = +0.05$ as the photospheric color for FGK-type stars with $J - K_s < 0.69$.

The observed $K_s - N$ colors of the M-type stars are systematically redder than those of the FGK stars, as well as the M-giant standards. We looked for independent confirmation that the turn-up in $K_s - N$ color for the coolest dwarfs is a real effect and not due to circumstellar material. We measure a color of $K_s - [11.6] = 0.33 \pm 0.06$ for the ∼12 Myr old M0 star GJ 803. Song et al. (2002) studied the spectral energy distribution (SED) of GJ 803 and concluded that the observed cold dust excess detected by *IRAS* at 60 μm does not contribute significant flux at 12 μm and that the *IRAS* 12 μm flux is consistent with the stellar photosphere. Our observed 11.6 μm flux (608 ± 32 mJy) agrees very well with the predicted photospheric flux (633 mJy at 11.6 μm), as well as the color-corrected *IRAS* 12 μm flux (537 ± 32 mJy). These observations confirm that the observed $K_s - [11.6]$ color for GJ 803 is photospheric and that the turn-up in $K_s - N$ color for M stars is real. It appears that none of the M-type stars has a statistically significant mid-IR excess. For the purposes of calculating upper limits on mid-IR excess, we fit a line to the mean $K_s - N$ colors for the KM-type stars with $J - K_s > 0.6$ (excluding the T Tauri star [PZ99] J161411) and model the M-type dwarf photosphere colors as $(K_s - N)_{phot} = -0.947 + 1.448(J - K_s)$ $(0.69 < J - K_s < 0.92)$.

We determine whether a star has detectable excess at *N* or 11.6 through calculating the excess as

$$E(N) = N - N_{phot} = N - K_s + (K_s - N)_{phot}, \quad (1)$$

$$\sigma^2[E(N)] = \sigma^2(N) + \sigma^2(K_s) + \sigma^2[(K_s - N)_{phot}]. \quad (2)$$

The contribution to the *N*-band excess from interstellar extinction will only become similar in size to our photometric

[3] Although not explicitly stated, the *K* photometry from Aumann & Probst (1991) appears to be on the CIT system, where 2MASS $K_s = K_{CIT} - 0.019$ (Carpenter 2001). The MIRAC *N*-band photometric system assumes $N = 0.00$ for Vega, whereas Aumann & Probst (1991) list $[12] = +0.01$ for Vega. We ignore any color terms in converting [12] to a predicted *N* magnitude and derive $K_s - N \simeq (K_{CIT} - [12]) - 0.01$.

TABLE 5

MEASURED PHOTOMETRY FOR OTHER STARS

Other Name (1)	*Hipparcos* Name (2)	Spectral Type (3)	K_s (mag) (4)	Band (5)	Predicted F_ν (mJy) (6)	Measured F_ν (mJy) (7)	$E(N)$ (mJy) (8)	Deviation (σ) (9)
Tuc-Hor Rejects								
HD 177171	HIP 93815	F7	3.81 ± 0.10[a]	*N*	1171	1236 ± 103	+65 ± 149	+0.4
HD 191869A[b]	HIP 99803A	F7	6.81 ± 0.02	*N*	74	87 ± 9	+13 ± 9	+1.5
HD 191869B[b]	HIP 99803B	...	6.86 ± 0.03	*N*	70	63 ± 14	−7 ± 14	−0.5
HD 202746	HIP 105441	K2	6.40 ± 0.02	*N*	107	116 ± 11	+9 ± 11	+0.8
HD 207129	HIP 107649	G0	4.12 ± 0.02[c]	*N*	880	837 ± 70	−43 ± 72	−0.6
PPM 366328	TYC 9129 1361 1	K0	7.61 ± 0.02	*N*	35	63 ± 24	+28 ± 24	+1.1
HD 208233[d]	HIP 108422	G8	6.75 ± 0.02	*N*	78	89 ± 14	+11 ± 14	+0.8
Upper Sco Members + FEPS								
[PZ99] J161411.0−230536	TYC 6793 819 1	K0	7.46 ± 0.03	*N*	48	273 ± 11	+225 ± 11	+20.3
ScoPMS 214	NTTS 162649−2145	K0	7.76 ± 0.02	*N*	42	37 ± 5	−5 ± 5	−1.0
ScoPMS 5	HD 142361	G3	7.03 ± 0.02[c]	*N*	60	58 ± 6	−2 ± 6	−0.4
HD 143006	HBC 608	G6/8	7.05 ± 0.03	*N*	134	648 ± 31	+514 ± 31	+16.5
HD 143006	HBC 608	G6/8	7.05 ± 0.03	11.6	104	640 ± 34	+536 ± 34	+15.7
[PZ99] J161318.6−221248	TYC 6213 306 1	G9	7.43 ± 0.02	*N*	45	32 ± 6	−13 ± 6	−2.2
β Pic Group Members								
GJ 799A	HIP 102141A	M4.5	5.70 ± 0.10[f]	11.6	202	259 ± 24	+57 ± 30	+1.9
GJ 799B	HIP 102141B	M4	5.70 ± 0.10[f]	11.6	202	260 ± 25	+58 ± 31	+1.9
GJ 803	HIP 102409	M0	4.53 ± 0.02	11.6	627	608 ± 32	−19 ± 34	−0.6
HD 181327	HIP 95270	F5/6	5.91 ± 0.03	*N*	169	200 ± 18	+31 ± 19	+1.7
HR 7329	HIP 95261	A0	5.01 ± 0.03	11.6	301	343 ± 31	+42 ± 32	+1.3
HR 7329	HIP 95261	A0	5.01 ± 0.03	*N*	387	466 ± 52	+79 ± 53	+1.5
CrA Off-Cloud Stars + FEPS								
RX J1853.1−3609	HD 174656	G6	7.28 ± 0.02	*N*	48	46 ± 4	−2 ± 4	−0.4
RX J1917.4−3756	SAO 211129	K2	7.47 ± 0.03	*N*	44	45 ± 4	+1 ± 4	+0.3
Sco-Cen Reject								
HD 113376[g]	HIP 63797	G3	6.70 ± 0.02	*N*	81	83 ± 9	+2 ± 9	+0.2
Other FEPS Targets								
HD 181321	HIP 95149	G5	4.93 ± 0.02	*N*	418	425 ± 21	+7 ± 22	+0.3
HD 191089	HIP 99273	F5	6.08 ± 0.03	11.6	113	132 ± 15	+19 ± 15	+1.3
HD 209253	HIP 108809	F6/7	5.39 ± 0.02	*N*	273	255 ± 21	−18 ± 22	−0.8
HD 216803	GJ 879	K4	3.81 ± 0.02[c]	*N*	1233	1027 ± 85	−206 ± 88	−2.3
HD 217343	HIP 113579	G3	5.94 ± 0.03	*N*	164	160 ± 8	−4 ± 9	−0.4
HD 984	HIP 1134	F5	6.07 ± 0.02	*N*	145	131 ± 14	−14 ± 14	−1.0

NOTES.—Col. (1): Other name. Col. (2): *Hipparcos* name. Col. (3): Spectral type (from SIMBAD unless otherwise noted). Col. (4): K_s magnitude from 2MASS (Cutri et al. 2003), unless otherwise noted. Col. (5): Measured MIRAC *N*-band flux. Col. (6): Predicted photospheric flux. Col. (7): Flux excess and uncertainty. Col. (8): Residual deviation = $E(N)/\sigma[E(N)]$.

[a] Star is saturated in 2MASS. We adopt the *V* magnitude from *Hipparcos* (ESA 1997) and the intrinsic $V - J$ and $J - K_s$ color for F7 stars from Kenyon & Hartmann (1995; converted to 2MASS system via Carpenter 2001), to calculate a rough K_s magnitude. We assume an uncertainty of 0.10 mag.

[b] Zuckerman et al. (2001a) call the pair HIP 99803 NE and SW. A = SE and B = NW.

[c] 2MASS photometry is saturated. We take the K_{CIT} magnitude from Aumann & Probst (1991) and transform it to the 2MASS system via equation (12) of Carpenter (2001).

[d] We cannot rule out HIP 108422 as a Tuc-Hor member based on its proper motion or the agreement between the calculated cluster parallax and *Hipparcos* trigonometric parallax. However, we conservatively exclude the star as a member at present, since no spectroscopic evidence of youth has been presented in the literature. If it is comoving with the Tucana nucleus, we predict a radial velocity of +3 km s^{-1}.

[e] A 0″.8 binary discovered by Ghez et al. (1993) and seen in MIRAC *K*-band images. MIRAC *N* and 2MASS K_s magnitudes are for unresolved pair.

[f] The 2MASS K_s magnitudes from Reid et al. (2002) appear to be at odds with the combined magnitude for A and B measured by Cutri et al. (2003), Nelson et al. (1986), and Probst (1983). The system is essentially an equal-brightness binary at optical bands as well as at *N*, so we split the 2MASS K_s magnitude evenly and adopt a generous 0.10 mag error. Spectral types are from Hawley et al. (1996).

[g] Rejected as a Sco-Cen member by Mamajek et al. (2002).

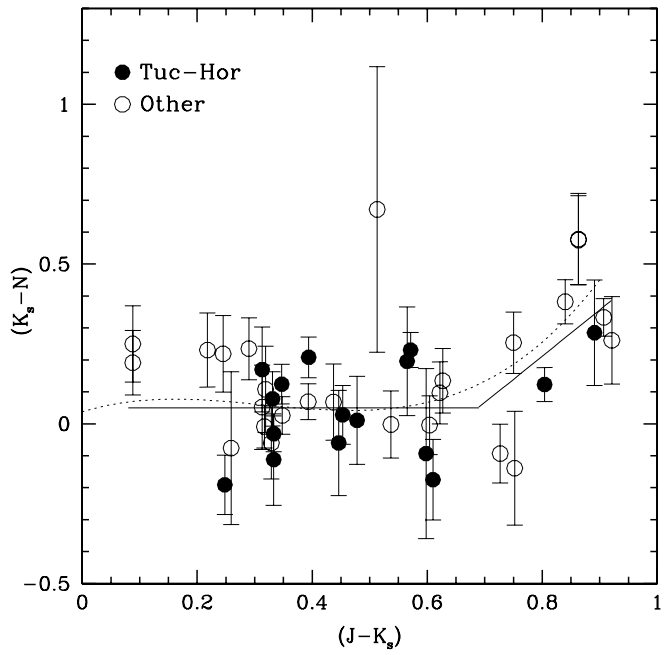

FIG. 1.—Color-color diagram for Tuc-Hor members (*filled circles*) and other stars observed in this study (*open circles*). Two stars (not members of Tuc-Hor) with significantly red $K_s - N$ colors are not shown (HD 143006 and J161411). *Solid line*: Our adopted photosphere color relation (§ 3). *Dashed line*: Smoothed fit to the $K_{\rm CIT} - [12]$ dwarf sequence of Kenyon & Hartmann (1995), where we calculate $K_s - N \simeq (K_{\rm CIT} - [12])_{\rm KH95} - 0.06$.

errors if $A_V \gtrsim 1-2$ mag; hence we can safely ignore extinction for the stars observed. We examined the residuals (defined as $E(N)/\sigma[E(N)]$) in order to identify statistically significant outliers (i.e., possible *N*-band excess stars). The ~5 Myr old Upper Sco members HD 143006 and [PZ99] J161411 (Preibisch & Zinnecker 1999) both stand out with definite *N*-band excesses ($\simeq$15–20 σ), and they are discussed further in Appendix B. There are two stars with positive 2–3 σ excesses (HIP 6485 and HIP 6856); however, there are three stars with 2–3 σ deficits (HIP 9685, GJ 879, and [PZ99] J161318). Hence, the weak excesses for HIP 6485 and HIP 6856 are probably statistical and not real. Excluding the two Upper Sco stars with strong *N*-band excesses, we find that 56% ± 12% of the excesses $E(N)$ are within 1 σ of zero and that 88% ± 15% are within 2 σ (uncertainties reflect Poisson errors). It does not appear necessary to introduce a nonzero uncertainty in the intrinsic $(K_s - N)_{\rm phot}$. If one wanted to force 68% of the residuals to be within ±1 σ and 95% to be within ±2 σ, than either $\sigma[(K_s - N)_{\rm phot}] \simeq 0.07-0.09$ mag, or our observational uncertainties are underestimated by ~40%. We searched for, and could not find, a plausible reason why our photometric errors would be underestimated by such a large amount. The observations of our standard stars certainly do not support a significant increase in our quoted photometric errors. More calibration observations are required to see if this dispersion can be attributed to actual structure in the intrinsic $K_s - N$ colors of normal dwarf stars as a function of spectral type.

Among the Tuc-Hor stars, only one star has an observed *N*-band flux ≥3 σ above that expected for stellar photosphere: HIP 6856 (3.0 σ excess). However, there is a Tuc-Hor member with a similarly sized flux *deficit* (HIP 9685; −2.9 σ), so it is difficult to claim that the excess for HIP 6856 is statistically significant. *We find that none of the 14* Tuc-Hor *members have an N-band excess more than 3 σ offset from the dwarf color relation*. We estimate a conservative upper limit to the *N*-band excess due to a hypothetical dust disk as 3 times the uncertainty in the flux excess ($\sigma[E(N)]$; given in col. [8] of Table 4).

4. DISK MODELS

Our survey was designed to be sensitive enough to detect the photospheres of young stars; hence we can place meaningful constraints on the census of even optically thin circumstellar disks in our target sample. We analyze the upper limits to possible mid-IR excess for the Tuc-Hor stars using three different models. The first model assumes a geometrically thin, optically thick disk with a large inner hole. The second model assumes emission from an optically thin disk of single-sized grains. The third model treats the hypothetical disks as a scaled-up version of the zodiacal dust disk in our solar system.

4.1. *Optically Thick Disk with Inner Hole*

Infrared and submillimeter observations of T Tauri stars in dark clouds show that roughly half are orbited by an optically thick circumstellar dust disk (see review by Beckwith 1999). While the stars in our sample are roughly an order of magnitude older (~30 Myr) than typical T Tauri stars in dark clouds (≤3 Myr), we can ask the question: If the Tuc-Hor stars have optically thick, geometrically thin disks, what is the minimum inner hole radius allowed by observations?

To answer this question for each star, we adopt the axisymmetric, geometrically thin, optically thick disk model of Adams et al. (1987) and follow the formalism of Beckwith et al. (1990). While we assume a face-on orientation ($\theta = 0$), our results are not strongly dependent on this assumption. We also assume that the disk is optically thick between $r_{\rm in}$ and $r_{\rm out}$ (300 AU is assumed for all models) and at all frequencies ($1 - e^{-\tau_\nu} \sim 1$). This is a safe assumption for T Tauri star disks in the wavelength regime probed in this study ($\lambda \leq 100$ μm; Beckwith et al. 1990).

Our *N*-band photometry alone allows us to rule out optically thick disks with inner hole radii of ~0.1 AU for the Tuc-Hor stars. Stronger constraints on inner disk radius for a hypothetical optically thick circumstellar disk can be calculated by including *IRAS* photometry. For *IRAS* point sources, we adopt 25, 60, and 100 μm fluxes and upper limits from the Faint Source Catalog (FSC; Moshir et al. 1990). Where no *IRAS* point source is detected, we adopt the *IRAS* Point Source Catalog (PSC) upper limits of 0.5 Jy (25 μm), 0.6 Jy (60 μm), and 1.0 Jy (100 μm) (IPAC 1986). For the brightest stars, the *IRAS* 60 and 100 μm data provide the strongest constraints on the existence of an optically thick disk, whereas for the fainter K-type and M-type stars, the MIRAC photometry provides the strongest constraint. *IRAS* did not map the region around HD 105; hence the inner hole radius we derive for this star is based only on the MIRAC *N*-band 3 σ upper limit. In Figure 2 we illustrate a typical example (HIP 1481) of how the MIRAC and *IRAS* photometry constrain the existence of optically thick disks around the Tuc-Hor stars. The values we derive for the minimum inner hole radius for a hypothetical optically thick disk are given in column (5) of Table 6. The median value of the minimum inner hole radius is ~0.3 AU (range: 0.1–7.9 AU). The *N*-band and *IRAS* upper limits place the strongest constraints on inner hole size for the luminous F stars ($r_{\rm in} \gtrsim 5$ AU) and the weakest constraints for the faint K/M stars ($r_{\rm in} \gtrsim 0.1$ AU). *The MIRAC and IRAS photometry easily rule*

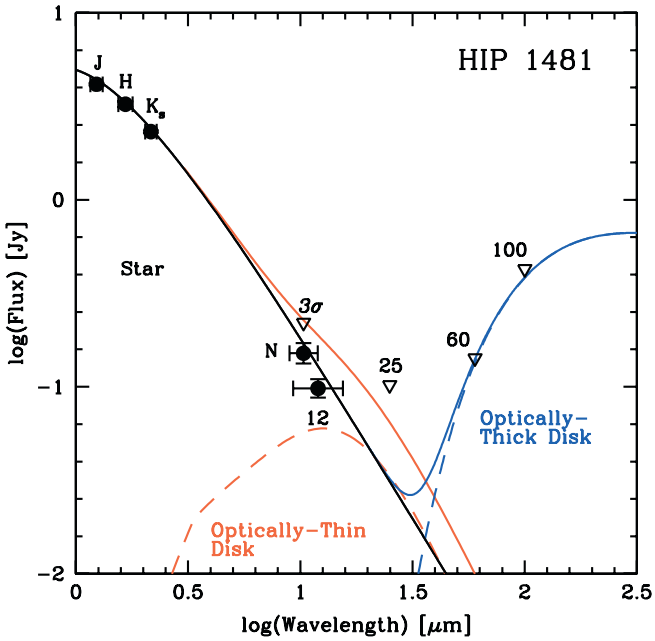

FIG. 2.—Optically thin and thick dust models fitted to the MIRAC and *IRAS* photometry for a typical Tuc-Hor star (HIP 1481). If the star has an optically thick disk, its inner hole radius must be greater than 1.8 AU (constrained by *IRAS* PSC 60 μm upper limits). The stellar SED is approximated here as a 6026 K blackbody. The optically thin disk model is conservatively matched to 3 times the uncertainty in the *N*-band excess $E(N)$. The kink in the SED for the optically thin model occurs at $\lambda = 2\pi\bar{a}$ because of our simple treatment of dust emissivity (§ 4.2).

out the existence of optically thick disks with inner hole radii of ~0.1 AU of the ~30 Myr old Tuc-Hor *stars*.

4.2. *Optically Thin Disk*

In the absence of circumstellar gas, a putative mid-IR excess around a ~30 Myr old star would be most likely to be due to an optically thin debris disk rather than an optically thick T Tauri–type disk. The stellar ages ($\sim 10^{7.5}$ yr) are orders of magnitude greater than the P-R drag timescale ($\sim 10^3$–10^4 yr) for typical interplanetary dust grains orbiting ~1 AU from a solar-type star. Small dust grains must be continually replenished by collisions of larger bodies or else they would be detectable only for astrophysically short timescales. Using a simple, single grain size model, we place upper limits on the amount of orbiting dust within several AU of the ~30 Myr old Tuc-Hor stars.

Circumstellar dust grains surrounding young main-sequence stars should most likely have radii somewhere between the scale of typical ISM grains (~0.01–1 μm; Mathis et al. 1977) and solar system zodiacal dust (~10–100 μm; Grün et al. 1985). Theoretically, an ensemble of dust grains produced from a collisional cascade of fragments is predicted to follow the equilibrium power-law size distribution (Dohnanyi 1969): $n(a)\,da = n_0 a^{-p}\,da$, where $p = 3.5$. Indeed this power-law distribution is observed for ISM grains (Mathis et al. 1977) and asteroids (Greenberg & Nolan 1989). With $p = 3.5$, most of the mass is in the largest (rarest) grains, but most of the surface area in the smallest (most common) grains. If the grain size distribution has a minimum cutoff, the mean grain size is calculated to be $\bar{a} = 5a_{\rm min}/3$ (e.g., Metchev et al. 2004). A limit on the minimum grain size $a_{\rm min}$ can be estimated from consideration of radiation pressure blowout (e.g., Artymowicz 1988):

$$a_{\rm min} = \frac{3L_* Q_{\rm pr}}{16\pi G M_* c\rho}, \qquad (3)$$

where L_* is the luminosity of the star, $Q_{\rm pr}$ is the radiation pressure efficiency factor averaged over the stellar SED, G is the Newtonian gravitational constant, M_* is the mass of the star, c is the speed of light, and ρ is the grain density (assumed to be 2.5 g cm^{-3}; Grün et al. 1985). The minimum grain size corresponds to the case where the ratio of the radiation pressure force to the stellar gravitational force is $F_{\rm rad}/F_{\rm grav} = 1$.

TABLE 6
MODEL PARAMETERS FOR TUC-HOR MEMBERS

Name (1)	π (mas) (2)	log $T_{\rm eff}$ (3)	log $(L/L_\odot)$ (4)	$r_{\rm hole}$ (AU) (5)	$\bar{a}$ (μm) (6)	$r_{\rm in} - r_{\rm out}$ (AU) (7)	Σ_0 (g cm^{-2}) (8)	$M_{\rm disk}$ ($M_\oplus$) (9)	log (L_d/L_*) (10)	$\mathcal{Z}$ (11)
HIP 490	24.9	3.776	+0.17	0.3	0.50	0.05–13.9	3.4E−06	7.8E−05	−3.25	2.6E+3
HIP 1481	24.4	3.780	+0.21	1.8	0.53	0.06–13.8	8.2E−06	1.9E−04	−2.89	6.4E+3
HIP 1910	21.6	3.585	−0.81	0.1	0.10	0.03–10.8	1.4E−05	1.9E−04	−2.20	2.9E+3
HIP 2729	21.8	3.643	−0.32	0.7	0.27	0.04–12.4	5.0E−06	9.2E−05	−2.80	2.1E+3
HIP 6485	20.3	3.744	−0.04	0.3	0.34	0.05–14.4	3.2E−06	7.7E−05	−3.10	2.0E+3
HIP 6856	26.9	3.707	−0.55	0.1	0.12	0.04–15.3	2.6E−06	7.1E−05	−2.85	1.1E+3
HIP 9685	21.2	3.829	+0.71	4.9	1.44	0.09–12.0	6.9E−06	1.2E−04	−3.45	7.5E+3
HIP 9892	19.9	3.752	−0.08	0.2	0.31	0.05–14.9	4.5E−06	1.2E−04	−2.91	3.0E+3
ERX 37 N	22.6	3.540	−0.89	0.1	0.14	0.02–8.6	8.3E−06	7.1E−05	−2.48	1.2E+3
HIP 105388	21.8	3.746	−0.16	0.2	0.26	0.05–15.3	5.4E−06	1.5E−04	−2.75	3.6E+3
HIP 105404	21.7	3.719	−0.21	0.2	0.26	0.04–14.6	6.4E−06	1.6E−04	−2.68	3.8E+3
HIP 107947	22.2	3.795	+0.38	2.1	0.75	0.06–13.0	6.3E−06	1.3E−04	−3.16	4.8E+3
HIP 108195	21.5	3.817	+0.91	7.9	2.40	0.11–11.7	1.0E−05	1.6E−04	−3.53	8.6E+3
HIP 116748A	21.6	3.746	−0.09	1.0	0.31	0.05–14.8	8.0E−06	2.1E−04	−2.65	5.0E+3
HIP 116748B	21.6	3.645	−0.46	0.2	0.19	0.04–13.0	1.4E−05	2.9E−04	−2.24	5.8E+3

NOTES.—Col. (1): Star name. Col. (2): Parallax. ERX 37 N parallax calculated via cluster parallax method; the other values are from *Hipparcos* (ESA 1997). Col. (3): Stellar effective temperature. Col. (4): Luminosity in solar units. Col. (5): Lower limits on inner hole radius for a hypothetical optically thick disk (§ 4.1). Col. (6): Mean calculated grain size, where $\bar{a} = 5a_{\rm min}/3$, where $a_{\rm min}$ is the blowout grain size (eq. [1]; § 4.2). Col. (7): Inner and outer radii for calculation of optically thin disk (§ 4.2). Col. (8): Disk surface mass density for optically thin disk model (§ 4.2); this is independent of radius for our adopted model with $\Sigma = \Sigma_0 r_{\rm AU}^{-p}$, $p = 0$. Col. (9): Upper limit on disk mass (in grains of size $\bar{a}$) for optically thin model (§ 4.2). Col. (10): Upper limit to fractional luminosity of scaled-up zodiacal dust model (§ 4.3). Col. (11): Upper limit to emitting area of scaled-up zodiacal dust model (in units of zodys, where 1 $\mathcal{Z} = 10^{21}$ cm^2; § 4.3).

TABLE 7
Effects of Changing Adopted Values on Model Output

Parameter (1)	Δr_{in} (2)	Δr_{out} (3)	$\Delta\Sigma_0$ (4)	ΔM_{dust} (5)	Case Name (6)
$\beta = 2$	$\times$(1.00–1.17)	$\times$(1.4–2.3)	/(1.3–0.26)	$\times$(1.5–21)	Crystalline case
$\beta = 1$	/(1.00–1.16)	/(1.4–2.3)	$\times$(1.2–0.24)	/(1.6–22)	Amorphous case
$\beta = 0$	/(1.01–1.74)	/(2.7–12)	$\times$(1.5–0.013)	/(4.7–10700)	Blackbody case
$\bar{a} \times 10$	/(1.01–1.73)	/(1.6–4.4)	$\times$(9.5–0.32)	$\times$(3.8–0.017)	...
$\bar{a} \times 100$	/(1.01–1.75)	/(1.6–7.1)	$\times$(95–2.7)	$\times$(38–0.054)	...
$p = 0.34$	No change	No change	$\times$(1.3–0.6)	/(1.5–2.8)	Zodiacal case
$p = 1$	No change	No change	$\times$(1.3–0.17)	/(4.7–26)	...
$p = 1.5$	No change	No change	/(1.1–21)	/(13–140)	Minimum mass solar nebula case

Notes.—Col. (1): Model parameter. Cols. (2)–(5): Range of factors acted upon model values in Table 6 if parameter in col. (1) is adopted. Col. (6): Case name.

For this calculation we assume the geometric optics case where $Q_{pr} = 1$. For the idealized grain orbiting the Sun at 1 AU, we calculate $a_{min} = 0.2$ μm and $\bar{a} = 0.4$ μm. The grain size lower limit may be larger if the momentum imparted by stellar winds dominates radiation pressure. The minimum grain size will be somewhat lower if we calculate Q_{pr} using Mie theory and stellar SEDs instead of adopting the geometric optics case. Highlighting the uncertainty in this calculation, we note that the value of $\bar{a}$ that we calculate for the Sun is $\sim 10^2$ times smaller than the mean interplanetary dust particle orbiting in the Earth's vicinity (Grün et al. 1985). This is largely due to a complex interplay between P-R drag and collisions. Increasing the cross-section of dust particles in the solar system zodiacal dust cloud by $\sim 10^4$ (i.e., comparable to what we are sensitive to in Tuc-Hor; see § 4.3) will decrease the collision timescale and correspondingly decrease the mean particle size to comparable to the blowout grain size (Dominik & Decin 2003).

We model the thermal emission from an optically thin disk of single-sized dust grains of radius $\bar{a}$ orbiting in an annulus between inner radius r_{in} and outer radius r_{out}. Spherical grains emit thermally at a temperature T_d, where the incident energy flux from the star is equal to the isotropically emitted output energy flux of the grain. We approximate the emissivity ϵ_λ of the single-sized dust grains by using the simple model of Backman & Paresce (1993): emissivity $\epsilon_\lambda = 1$ for $\lambda < 2\pi a$, and $\epsilon_\lambda = (\lambda/2\pi a)^{-\beta}$ for longer wavelengths, where we assume $\beta = 1.5$. Our adopted value of β is similar to that observed for zodiacal dust (see Fig. 2 of Fixsen & Dwek 2002) and ISM grains (Backman & Paresce 1993). The mass opacity is calculated as $\kappa_\lambda = 3\epsilon_\lambda/4a\rho$. The optical depth of emission through the disk annulus is $\tau_\lambda = \Sigma\kappa_\lambda$, where Σ is the surface density of the disk in g cm^{-2}. We calculate the orbital distance from the star (r) of dust grains heated to temperature T using equation (5) of Wolf & Hillenbrand (2003). We verify that this relation is valid by comparing our calculations with Backman & Paresce (1993) for grains much larger than the Wien peak of incident light (blackbody case) and for grains much smaller than the Wien peak of incident light (e.g., ISM grains). For the Tuc-Hor stars, the Wien peak of incident starlight is comparable to $\bar{a}$. We assume a flat mass surface density profile ($\Sigma = \Sigma_0 r_{AU}^{-p}$; $p = 0$), which is appropriate for a population of dust grains in circular orbits subject to P-R drag (see discussion in § 4.1 of Wolf & Hillenbrand 2003 and references therein). This predicted power law is close to what is observed for the zodiacal dust disk in our own solar system ($p = 0.34$; Kelsall et al. 1998).

Where exactly to define the inner and outer radii of a hypothetical dust disk requires some basic modeling. Among the Tuc-Hor stars, 90% of the thermal emission from our hypothetical disk model at N band comes from within $\approx$(1.5–2.2)r_W of the star, where r_W is the radius at which the dust is at the Wien temperature (T_W) for the isophotal wavelength of the N-band filter, and $T_W = 2898\lambda_{\mu m}^{-1}[5/(\beta + 5)]$ (eq. [6.9] of Whittet 2003). For simplicity, we adopt a consistent definition of the outer radius for all stars as $2r_W$. Beyond $2r_W$, the hypothetical dust disk contributes negligible flux ($\lesssim$10%) to what is observed in the N-band filter. Approximately 50% of the thermal emission observed in N band from a hypothetical dust disk comes from within $\lesssim$(0.4–0.5)r_W of the star. For r_{in}, we adopt the radius for which the grain temperature is 1400 K—approximately the silicate dust sublimation limit. The temperatures of the inner edges of typical T Tauri star disks appear to be near this value (Muzerolle et al. 2003). For the Tuc-Hor stars, $r_{in} \sim 0.05$ AU and $r_{out} \sim 10$–15 AU. Hence we are most sensitive to dust at orbital radii comparable to our inner solar system.

Results for a typical set of fitted model parameters for our optically thin disk model are illustrated in Figure 2. Our calculations suggest that the survey was sensitive to dust disk masses of $\sim 2 \times 10^{-6}$ $M_\oplus$ ($\sim 10^{22}$ g) in a single-sized dust grain population (of uniform size $\bar{a}$, typically 0.1–2 μm). Our optically thin model puts upper limits of $\Sigma_0 \simeq 10^{-6}$ to 10^{-5} g cm^{-2} on the surface density of micron-sized dust grains in the $\sim$0.1-10 AU region around the Tuc-Hor stars. *For the masses and surface densities quoted, we assume that all of the mass is in dust grains of size $\bar{a}$.* In order to convey how sensitive our assumptions are for our final results, we show the effects of changing various parameters on our results in Table 7. The dust disk masses that we calculate are similar to those found by other studies (Chen & Jura 2001; Metchev et al. 2004), which also use the single grain size approximation. The dust mass surface density upper limits that we calculate are $\sim 10^{-7}$ to 10^{-6} times that of the solids in the minimum-mass solar nebula (Weidenschilling 1977); however, we are not sensitive to bodies much larger than the wavelength of our observations or to gas.

4.3. *Single-Temperature Zody Disk*

Another simple model to apply to our data is that of a scaled-up version of the terrestrial-zone zodiacal dust cloud in our own solar system. Although the detailed zodiacal dust model for the inner solar system is quite complex (Kelsall et al. 1998), it can also be approximated by a single-temperature blackbody

($T = 260$ K) with bolometric luminosity $8 \times 10^{-8}\ L_{\odot}$ (Gaidos 1999). This luminosity and temperature imply an equivalent surface area of 5×10^{-6} AU$^2 \simeq 1 \times 10^{21}$ cm^2. Gaidos (1999) defines this area as 1 "zody" (1 $\mathcal{Z}$). The unit is useful for comparing relative amounts of exozodiacal dust between the Sun and other stars.

With none of our stars having statistically significant *N*-band excesses, we calculate upper limits to the number of zodys present using 3 times the uncertainty in the excess measurement, assuming $T_d = 260$ K and blackbody emission from large grains (i.e., analogous to the situation for the solar system zodiacal dust disk). An upper limit on the fraction of grain thermal emission to stellar emission ($f_d = L_{\rm dust}/L_*$) was also calculated for each star using these assumptions. While the MIRAC photometry is capable of detecting $\sim$4000 $\mathcal{Z}$ disks at $T = 260$ K [equivalent $\log(f_d) < -2.9$] around the Tuc-Hor members observed, no convincing mid-IR excesses were detected.

For completeness, we note that the fraction of disk luminosity to stellar luminosity ($f_d = L_d/L_*$) has been observed to fall off as $f_d \propto {\rm age}^{-1.76}$ (Spangler et al. 2001). The disk fractional luminosity is predicted to follow $f_d \propto {\rm age}^{-2}$ if the observed amount of dust is proportional to the collision frequency of large particles and P-R drag is the dominant dust removal mechanism. Recently, Dominik & Decin (2003) have argued that for the very luminous debris disks that have been detected so far, the collision timescales are much shorter than the P-R drag timescales, all the way down to the blowout grain size. For this collision-dominated scenario, Dominik & Decin (2003) predict that the dust luminosity evolves as $f_d \propto {\rm age}^{-1}$. While these models ignore effects such as, e.g., gravitational perturbations or ejections of dust-producing planetesimals by planets (which likely had an enormous effect on the early evolution of the asteroid belt in our solar system), they provide simple, physically plausible models with which to compare observations.

If one were to take the solar system zodiacal dust disk [$\log(f_d) \simeq -7.1$ at $\log({\rm age_{yr}}) = 9.66$] and scale it backward in time according to Spangler et al.'s relation ($f_d \propto {\rm age}^{-1.76}$) or the theoretical P-R drag–dominated evolution ($f_d \propto {\rm age}^{-2}$), one would predict at age 30 Myr zodiacal dust disks with $\log(f_d) \simeq -3.3$ (6900 $\mathcal{Z}$) or $\log(f_d) \simeq -2.7$ (23,000 $\mathcal{Z}$), respectively. Hence, for the simple model of collisionally replenished, P-R drag–depleted disks, *we should have easily detected the solar system's zodiacal dust disk at age 30 Myr.* For the empirical relation (Spangler et al. 2001), we could have detected the Sun's zody disk around most (13/15) of the $\sim$30 Myr old Tuc-Hor stars in our sample. Backward extrapolation of the Sun's zodiacal dust disk luminosity using Dominik & Decin's relation for collisionally dominated disks would yield $\log(f_d) \simeq -4.9$ (150 $\mathcal{Z}$). Such a disk would not have been detectable in our survey, consistent with our null result. *If* analogs of the Sun's zodiacal dust disk are common around 30 Myr old stars, f_d must evolve as a shallower power law (<1.65) than either Spangler et al.'s empirical relation or the P-R drag–dominated dust depletion model.

5. DISCUSSION

In Figure 3 we plot the incidence of *N*-band excess versus stellar age for samples of low-mass stars. While $\sim$80% of $\sim$1 Myr old stars have in Taurus have *N*-band excesses (Kenyon & Hartmann 1995), only $\sim$10% of $\sim$10 Myr old stars in the TW Hya association and β Pic moving group show comparable excess emission (Jayawardhana et al. 1999; Weinberger et al. 2003a, 2003b). Of these $\sim$10 Myr old stars, only a few are known to have optically thick disks (TW Hya, Hen 3-600), while the others are optically thin disks. Our survey imaged a small number ($N = 5$) of Upper Sco members ($\sim$5 Myr old) as well, among which two have clear *N*-band excesses. By an age of $\sim$30 Myr, we find that *N*-band excesses due to optically thick *or* optically thick disks are rare ($\lesssim$7%). Excluding the $\sim$10 Myr old star β Pic, Aumann & Probst (1991) find only one star (ζ Lep) among a sample of 548 field AFGK stars ($\approx$0.2%) with a convincing 12 μm excess. These results seem to imply that *dust appears to be efficiently removed from less than 5 to 10 AU of young stars on timescales similar to that of the cessation of accretion*. While accretion terminates over a wide range of ages ($\sim$1–10 Myr; Haisch et al. 2001a; L. A. Hillenbrand et al. 2004, in preparation), the *duration* of the transition from optically thick to optically thin has been observed to be remarkably short ($\sim 10^5$ yr; Skrutskie et al. 1990; Wolk & Walter 1996).

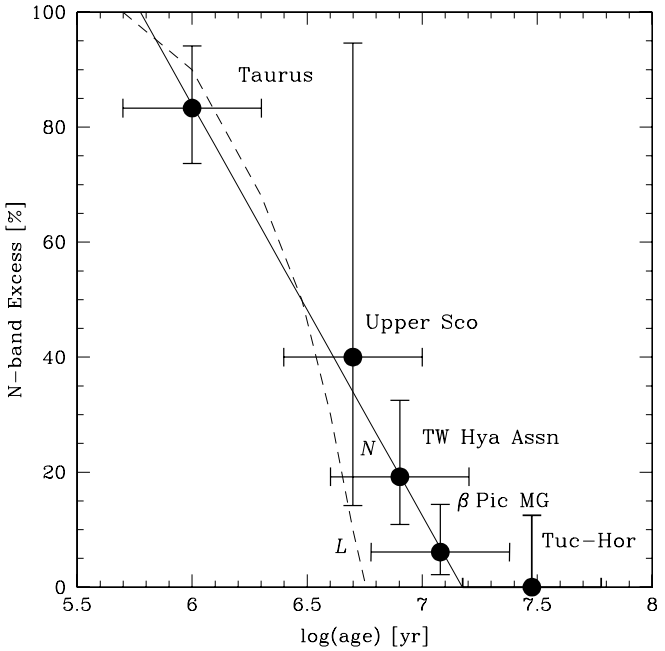

FIG. 3.—*N*-band excess vs. age for stellar samples of varying ages. Data are plotted for the following samples: Taurus-Auriga (Kenyon & Hartmann 1995), TW Hya association (Jayawardhana et al. 1999; Weinberger et al. 2003a), β Pic group (Weinberger et al. 2003b) and Upper Sco and Tuc-Hor (both in this study). Data from the *IRAS* study of AFGK-type field stars by Aumann & Probst (1991) show that *N*-band excesses among mostly older ($\gtrsim$100 Myr) field stars are extraordinarily rare ($\sim$0.2%). *Dashed line*: *L*-band disk fraction measured by Haisch et al. (2001a). *Solid line*: *N*-band disk fraction for the four youngest groups. It appears that *N*-band excesses are only detectable for timescales marginally longer than that of *L*-band excesses; however, the statistics are still poor. Note that in the TW Hya association, there exists a mix of optically thick and thin disks, while in the β Pic group, all of the known disks are optically thin.

Gravitational perturbations of small planetesimals ($\sim$0.1–100 km radius) by growing planetary embryos ($\sim$2000 km radius) can theoretically cause collisional cascades of dust grains that produce observable mid-IR signatures (Kenyon & Bromley 2004). Simulations show that when the largest planetary embryos reach radii of $\sim$3000 km, the population of dust-producing $\sim$0.1–100 km sized planetesimals in the planet-forming zone becomes collisionally depleted and *N*-band excesses become undetectable. The timescale over which the *N*-band excess would be detectable during this phase of terrestrial planet formation is of order $\sim$1 Myr. With a larger

sample size (e.g., FEPS *Spitzer* Legacy survey), one might be able to probe whether this is occurring around stars at age $\sim$30 Myr. With 10% of $\sim$10 Myr old stars having detectable *N*-band excesses (Jayawardhana et al. 1999; Weinberger et al. 2003a, 2003b), we may be witnessing the signature from runaway protoplanet growth in the terrestrial planet zone (Kenyon & Bromley 2004). This would agree with the isotopic evidence in our own solar system that Moon to Mars sized protoplanetary embryos accreted within the first $\sim$10–20 Myr (Kleine et al. 2002, 2003), ultimately leading to the formation of the Earth-Moon system.

6. CONCLUSIONS

We have undertaken a mid-IR survey of 14 young stars in the nearby $\sim$30 Myr old Tuc-Hor association in order to search for emission from warm circumstellar disks. No excess emission at 10 μm was detected around any Tuc-Hor members. If optically thick disks do exist around these stars, their inner holes must be large (range: 0.2–5.8 AU). Combining our photometric results with optically thin dust disk models, we place the following physical constraints on dust orbiting within $\sim$10 AU of these $\sim$30 Myr old stars: fractional disk luminosities of $L_{\rm dust}/L_* < 10^{-2.9}$ and dust-emitting surface areas of less than 4000 times that of the inner solar system zodiacal dust. The disk masses of micron-sized dust grains with orbital radii between the silicate dust sublimation point and $\sim$10 AU must be less than $\sim 10^{-6}\,M_\oplus$. The photometric upper limits also suggest that the upper limit on the surface density of micron-sized grains is $\sim 10^{-7}$ g cm^{-2}. These results imply that inner disks dissipate on timescales comparable to the cessation of accretion.

E. E. M. gratefully acknowledges a NASA Graduate Student Fellowship (NGT5-50400) for support. E. E. M. and M. R. M. are supported by the *Spitzer Space Telescope* Legacy Science Program, provided by NASA through contract 1224768 administered by the Jet Propulsion Laboratory, California Institute of Technology, under NASA contract 1407. M. C. thanks NASA for supporting his participation in this work through JPL contract 1224634 with UC Berkeley. MIRAC is supported through SAO and NSF grant AST 96-18850. BLINC is supported through the NASA Navigator program. For their technical support during the MIRAC runs at Magellan, we would like to thank Brian Duffy (Steward Observatory) and the staff of the Las Campanas Observatory: Emilio Cerda, Oscar Dulhalde, Patricio Jones, Gabriel Martin, Mauricio Navarette, Hernan Nuñez, Frank Perez, Hugo Rivera, Felipe Sanchez, Skip Schaller, and Geraldo Valladares. We thank Lissa Miller, Nick Siegler, and Lynne Hillenbrand for critiquing drafts of this manuscript.

APPENDIX A

MIRAC PHOTOMETRIC CALIBRATION

With a significant body of MIRAC-BLINC observations acquired during the 2001–2003 observing runs at Magellan I, it was decided to calculate the photometric attributes of commonly used MIRAC bands on the Cohen-Walker-Witteborn (CWW) system of absolute infrared calibration (e.g., Cohen et al. 2003b and references therein). The photometric standard system for previously published MIRAC studies is given in Appendix 2 of the MIRAC3 User's Manual (Hoffmann & Hora 1999).

Relative spectral responses (RSRs) for each combination of filter and window were constructed. The throughput chain consists of the following groups of components: atmosphere, telescope optics, BLINC optics, MIRAC optics, and the MIRAC detector. The complete throughput equation consists of the following components multiplied together: atmosphere, three aluminum mirrors (Magellan), Dewar window (KRS 5 or KBr), KBr lens (in BLINC), five gold mirrors (three in BLINC, two in MIRAC), filter, and the Si:As array. Most of the MIRAC observations were taken in just four of the 17 filters currently available in the three MIRAC filter wheels: *L*, *N*, 11.6, and Q_s, and these were the filters we absolutely calibrated. For each MIRAC filter, we list a manufacturer's name, mean filter wavelength (λ_0), bandwidth ($\Delta\lambda/\lambda$; defined as the FWHM of the normalized transmission curve divided by the mean wavelength), and the temperature at which the filter profile was measured (or extrapolated). The transmission profiles for the filters are plotted in Figure 4. While we list *mean* filter wavelengths (λ_0) in this discussion, the *isophotal* wavelengths ($\lambda_{\rm iso}$) are given in Table 8.

The *L* filter (OCLI "Astro *L*"; $\lambda_0 = 3.84$ μm, $\Delta\lambda/\lambda = 16.2\%$, 77 K) is the same one used in all previous and current MIRAC *L*-band observations, and the transmission curve is plotted in Figure A2.2 of Hora (1991). The *N* filter (OCLI code W10773-8; $\lambda_0 = 10.75$ μm, $\Delta\lambda/\lambda = 47.2\%$, ambient) was purchased in 1994 in preparation for comet Shoemaker-Levy 9 observations and has been in use ever since. Pre-1994 MIRAC observations employed a slightly bluer wideband *N* filter whose characteristics we only present here for completeness (OCLI code W10575-9; $\lambda_0 = 10.58$ μm, $\Delta\lambda/\lambda = 45.8\%$, ambient). The narrow 11.6 μm filter (OCLI "Astronomy R"; $\lambda_0 = 11.62$ μm, $\Delta\lambda/\lambda = 9.5\%$, extrapolated to 5 K) has been used since MIRAC was commissioned (Hora 1991). Its transmission curve includes the effects of a BaF_2 blocker, and it is the only filter of the four for which we were able to linearly extrapolate its transmission characteristics to the detector's operating temperature (5 K; data at ambient and 77 K were available). The Q_s or "*Q*-short" filter has also been used for the lifetime of MIRAC, and its characteristics are only currently known at ambient temperature: $\lambda_0 = 17.50$ μm, $\Delta\lambda/\lambda = 10.6\%$.

We followed Cohen et al. (1999) in using PLEXUS (Clark 1996) to assess mean, site-specific atmospheric transmission. Transmission curves for KRS 5 and KBr were taken from the Infrared Handbook (Wolfe & Zissis 1985). We used a KRS 5 window during the 2001 August and 2002 May runs and a KBr window for the 2002 August and 2003 March runs. The reflectivities of the gold and aluminum mirrors were assumed to be flat in the wavelength range of interest (2–20 μm). The quantum efficiency for the MIRAC doped-silicon blocked impurity band (BIB) array was taken from Stapelbroek et al. (1995), following Hoffmann et al. (1998). The zero-magnitude attributes of the MIRAC filter systems are given in Table 8. Standard-star fluxes on the CWW system for the four primary MIRAC filters (with the KRS 5 Dewar window) are given in Table 9. When the KBr Dewar window is used on MIRAC-BLINC, the standard-star fluxes are nearly identical (to within $<$7% of the quoted flux uncertainties), so the same fluxes and magnitudes can be safely adopted. The flux densities in Tables 4 and 5 are referenced to this system.

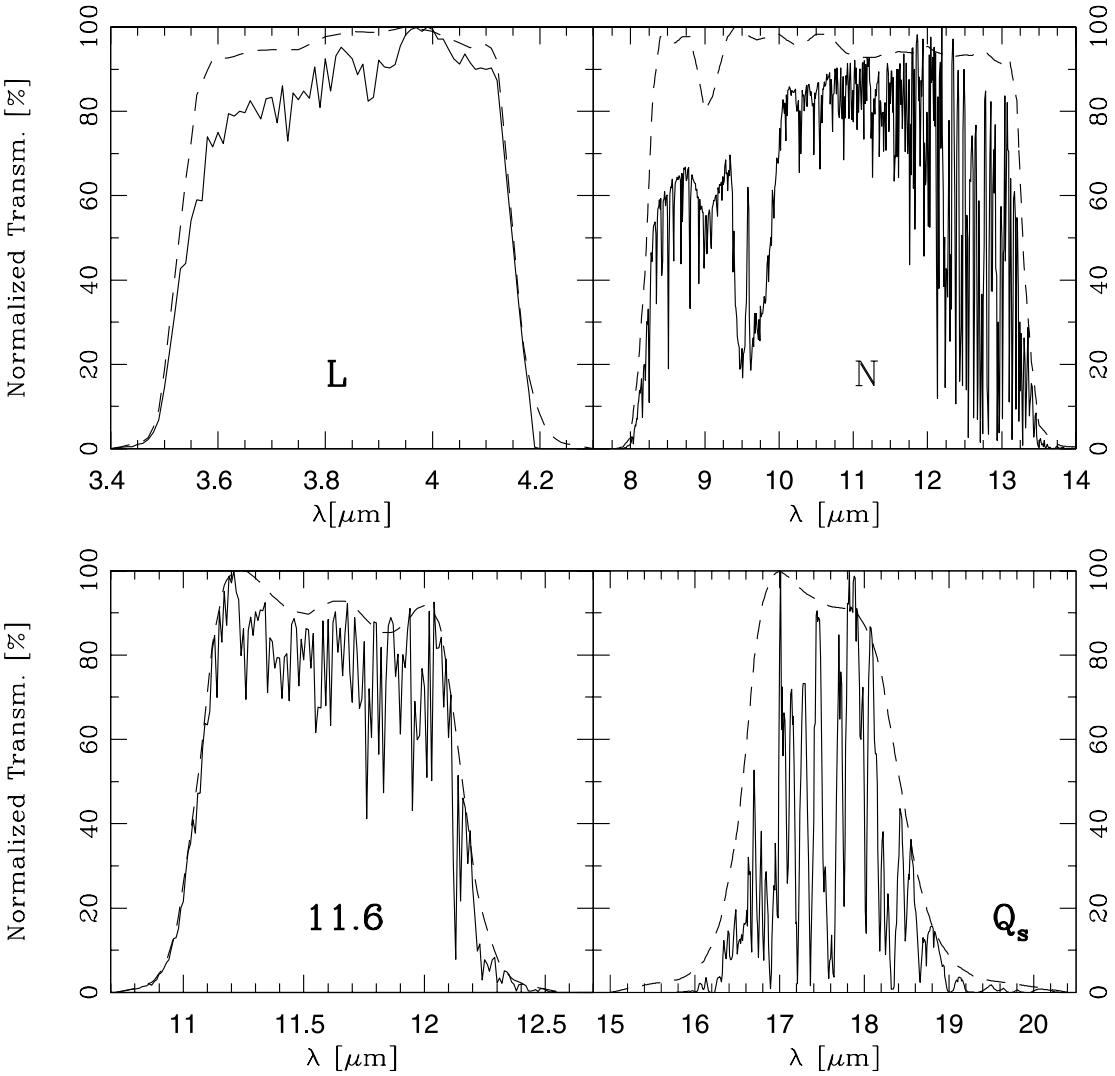

FIG. 4.—Transmission profiles for the MIRAC *L*, *N*, 11.6, and Q_s filters. *Dashed lines*: Normalized filter transmission profiles. *Solid lines*: RSR curves (details given in Appendix A) representing the product of transmissions for the filters, detector, optics, KRS 5 Dewar window, and atmosphere. The RSRs were used for absolutely calibrating MIRAC on the CWW system.

TABLE 8

ZERO-MAGNITUDE ATTRIBUTES OF MIRAC PHOTOMETRIC BANDS

MIRAC Band (1)	λ_{iso} (μm) (2)	Bandwidth (μm) (3)	In-Band Flux (W cm^{-2}) (4)	F_λ(iso) (W cm^{-2} μm^{-1}) (5)	Bandwidth (Hz) (6)	F_ν(iso) (Jy) (7)	ν(iso) (Hz) (8)
L	3.844	0.5423	2.631E−15	4.852E−15	1.102E+13	238.8	7.793E+13
Uncertainty	0.018	0.0037	1.609%	8.469E−17	6.820E+10	4.1	7.361E+11
N	10.35	3.228	3.263E−16	1.011E−16	8.760E+12	37.25	2.946E+13
Uncertainty	0.05	0.022	1.632%	1.789E−18	4.170E+10	0.60	2.416E+11
11.6	11.57	0.8953	5.816E−17	6.496E−17	2.006E+12	29.00	2.592E+13
Uncertainty	0.08	0.0135	2.110%	1.686E−18	2.149E+10	0.61	2.827E+11
Q_s	17.58	0.9130	1.123E−17	1.230E−17	8.834E+11	12.72	1.706E+13
Uncertainty	0.14	0.0185	2.494%	3.951E−19	1.263E+10	0.32	2.171E+11

NOTES.—Col. (1): Name of MIRAC band. Col. (2): Isophotal wavelength. Col. (3): Wavelength bandwidth of RSR. Col. (4): In-band flux for zero-magnitude star. Col. (5): Isophotal monochromatic intensity (wavelength units). Col. (6): Frequency bandwidth of RSR. Col. (7): Isophotal monochromatic intensity (frequency units). Col. (8): Isophotal frequency. Note that the stated quantities assume that a KRS 5 Dewar window is used. If the KBr Dewar window is used, the values are nearly identical. For KBr, every stated value is within 5% of the stated uncertainty for the *L*, 11.6, and Q_s bands, and within 36% of the stated uncertainty for *N* band.

TABLE 9

PREDICTED MIRAC STANDARD-STAR FLUXES ON CWW SYSTEM

HD Name (1)	Alternate Name (2)	Band (3)	Magnitude (4)	Uncertainty (5)	F_λ (W cm^{-2} μm^{-1}) (6)	Uncertainty (W cm^{-2} μm^{-1}) (7)	F_ν (mJy) (8)	Uncertainty (mJy) (9)	Uncertainty (%) (10)
1522.....	ι Cet	L	0.800	0.022	2.32E−15	4.99E−17	1.14E+05	2.46E+03	2.15
		N	0.807	0.021	4.81E−17	9.98E−19	1.77E+04	3.68E+02	2.08
		11.6	0.772	0.026	3.19E−17	9.01E−19	1.42E+04	4.02E+02	2.83
		Q_s	0.775	0.030	6.02E−18	2.08E−19	6.23E+03	2.16E+02	3.46
12929.....	α Ari	L	−0.762	0.021	9.79E−15	2.01E−16	4.82E+05	9.88E+03	2.05
		N	−0.754	0.020	2.02E−16	4.00E−18	7.46E+04	1.47E+03	1.98
		11.6	−0.789	0.025	1.34E−16	3.70E−18	6.00E+04	1.65E+03	2.75
		Q_s	−0.787	0.030	2.54E−17	8.63E−19	2.62E+04	8.93E+02	3.40
29139.....	α Tau	L	−3.045	0.021	8.01E−14	1.62E−15	3.94E+06	7.99E+04	2.03
		N	−3.013	0.020	1.62E−15	3.21E−17	5.97E+05	1.18E+04	1.98
		11.6	−3.074	0.025	1.10E−15	3.03E−17	4.92E+05	1.35E+04	2.75
		Q_s	−3.058	0.029	2.06E−16	6.91E−18	2.13E+05	7.14E+03	3.36
45348.....	α Car	L	−1.289	0.019	1.59E−14	3.04E−16	7.83E+05	1.50E+04	1.91
		N	−1.309	0.020	3.38E−16	6.53E−18	1.24E+05	2.41E+03	1.94
		11.6	−1.307	0.025	2.17E−16	6.03E−18	9.67E+04	2.69E+03	2.78
		Q_s	−1.307	0.029	4.10E−17	1.37E−18	4.24E+04	1.42E+03	3.35
48915.....	α CMa	L	−1.360	0.017	1.70E−14	2.96E−16	8.36E+05	1.46E+04	1.75
		N	−1.348	0.018	3.50E−16	6.19E−18	1.29E+05	2.28E+03	1.77
		11.6	−1.346	0.023	2.24E−16	5.82E−18	1.00E+05	2.60E+03	2.59
		Q_s	−1.341	0.027	4.23E−17	1.36E−18	4.38E+04	1.41E+03	3.21
81797.....	α Hya	L	−1.362	0.019	1.70E−14	3.19E−16	8.37E+05	1.57E+04	1.88
		N	−1.309	0.019	3.38E−16	6.39E−18	1.24E+05	2.36E+03	1.89
		11.6	−1.351	0.027	2.25E−16	6.59E−18	1.01E+05	2.94E+03	2.92
		Q_s	−1.350	0.030	4.26E−17	1.46E−18	4.41E+04	1.51E+03	3.42
106849.....	ϵ Mus	L	−1.594	0.029	2.11E−14	5.83E−16	1.04E+06	2.87E+04	2.77
		N	−1.647	0.027	4.61E−16	1.17E−17	1.70E+05	4.32E+03	2.54
		11.6	−1.708	0.031	3.13E−16	1.01E−17	1.40E+05	4.53E+03	3.24
		Q_s	−1.700	0.039	5.89E−17	2.42E−18	6.09E+04	2.50E+03	4.10
108903.....	γ Cru	L	−3.299	0.039	1.01E−13	3.71E−15	4.99E+06	1.83E+05	3.66
		N	−3.354	0.038	2.22E−15	7.95E−17	8.18E+05	2.93E+04	3.58
		11.6	−3.413	0.041	1.51E−15	6.13E−17	6.73E+05	2.74E+04	4.07
		Q_s	−3.403	0.043	2.83E−16	1.27E−17	2.92E+05	1.31E+04	4.49
128620.....	α Cen A	L	−1.562	0.018	2.04E−14	3.58E−16	1.01E+06	1.76E+04	1.75
		N	−1.564	0.018	4.27E−16	7.57E−18	1.57E+05	2.79E+03	1.77
		11.6	−1.565	0.023	2.75E−16	7.13E−18	1.23E+05	3.18E+03	2.60
		Q_s	−1.566	0.027	5.20E−17	1.67E−18	5.38E+04	1.73E+03	3.21
133216.....	σ Lib	L	−1.565	0.025	2.05E−14	5.00E−16	1.01E+06	2.46E+04	2.44
		N	−1.619	0.022	4.49E−16	9.79E−18	1.66E+05	3.61E+03	2.18
		11.6	−1.680	0.028	3.05E−16	9.03E−18	1.36E+05	4.03E+03	2.96
		Q_s	−1.670	0.036	5.73E−17	2.23E−18	5.92E+04	2.30E+03	3.89
135742.....	β Lib	L	2.874	0.019	3.44E−16	6.39E−18	1.69E+04	3.14E+02	1.86
		N	2.899	0.019	7.00E−18	1.32E−19	2.58E+03	4.85E+01	1.88
		11.6	2.904	0.025	4.48E−18	1.23E−19	2.00E+03	5.49E+01	2.75
		Q_s	2.915	0.029	8.40E−19	2.78E−20	8.68E+02	2.88E+01	3.32
150798.....	α TrA	L	−1.337	0.022	1.66E−14	3.50E−16	8.18E+05	1.72E+04	2.11
		N	−1.329	0.021	3.44E−16	6.99E−18	1.27E+05	2.58E+03	2.03
		11.6	−1.364	0.026	2.28E−16	6.38E−18	1.02E+05	2.85E+03	2.80
		Q_s	−1.361	0.030	4.31E−17	1.48E−18	4.46E+04	1.53E+03	3.44
167618.....	η Sgr	L	−1.731	0.022	2.39E−14	5.08E−16	1.18E+06	2.50E+04	2.13
		N	−1.696	0.021	4.82E−16	9.86E−18	1.78E+05	3.63E+03	2.04
		11.6	−1.753	0.026	3.26E−16	9.13E−18	1.46E+05	4.08E+03	2.80
		Q_s	−1.786	0.031	6.37E−17	2.25E−18	6.59E+04	2.33E+03	3.53
216956.....	α PsA	L	1.002	0.019	1.93E−15	3.62E−17	9.49E+04	1.78E+03	1.88
		N	1.001	0.019	4.02E−17	7.65E−19	1.48E+04	2.82E+02	1.90
		11.6	1.004	0.025	2.58E−17	7.11E−19	1.15E+04	3.18E+02	2.76
		Q_s	1.008	0.029	4.86E−18	1.62E−19	5.02E+03	1.67E+02	3.33

NOTES.—All stated quantities assume that a KRS 5 Dewar window is used. If the KBr window is used, the values are nearly identical (to within 7% of the stated uncertainties).

APPENDIX B

COMMENTS ON INDIVIDUAL SOURCES

The only young stars in our survey to show a significant *N*-band excess were the T Tauri stars HD 143006 and [PZ99] J161411.0−230536, both members of the ∼5 Myr old Upper Sco OB subgroup. Both stars are targets in the FEPS *Spitzer* Legacy Science Program, but only HD 143006 was previously known to possess a circumstellar disk. Both were detected by *IRAS*, and the MIRAC *N*-band fluxes are consistent with the color-corrected 12 μm measurements in the *IRAS* FSC (Moshir et al. 1990). Here we discuss these stars in more detail.

B1. [PZ99] J161411.0−230536

J161411 is a K0-type weak-lined T Tauri [EW(Hα) = 0.96 Å] star discovered by Preibisch et al. (1998). In a spectroscopic survey to identify new members of Upper Sco (E. E. Mamajek, M. R. Meyer, & J. Liebert 2004, in preparation), the authors obtained a red, low-resolution spectrum of J161411 in 2000 July that shows an asymmetric Hα feature with blueshifted emission and redshifted absorption [net EW(Hα) = 0.36 Å]. We confirm the strong lithium absorption [EW(Li λ6707) = 0.45 Å] observed by Preibisch et al. (1998). The UCAC2 proper motion (Zacharias et al. 2004) for J161411 is consistent with membership in the Upper Sco subgroup. The $K_s - N$ color (=2.1) is similar to that of classical T Tauri stars in Taurus-Auriga (Kenyon & Hartmann 1995). The photometric and spectroscopic evidence suggest that this ∼5 Myr old, ∼1 $M_\odot$ star is actively accreting from a circumstellar disk.

B2. HD 143006

HD 143006 is a G5 Ve (Henize 1976) T Tauri star with strong Li absorption [EW(Li λ6707) = 0.24 Å; Dunkin et al. 1997]. The star is situated in the middle of the Upper Sco OB association, and its proper motion ($\mu_\alpha,\ \mu_\delta = -11,\ -20$ mas yr^{-1}; Zacharias et al. 2004) and radial velocity (−0.9 km s^{-1}; Dunkin et al. 1997) are indistinguishable from other association members (de Bruijne 1999). Several studies have classified HD 143006 as a distant G-type supergiant or "preplanetary nebula" (Carballo et al. 1992; Kohoutek 2001); however, we believe this is erroneous. If HD 143006 were indeed a supergiant at $d = 3.4$ kpc (Pottasch & Parthasarathy 1988), its tangential velocity would be ∼370 km s^{-1}—extraordinarily fast for a Population I star. The MIRAC *N* and 11.6 photometry agrees well with the data points in the SED for HD 143006 plotted in Figure 2 of Sylvester et al. (1996). The SED for HD 143006 and its optically thick disk is well studied from 0.4 to 1300 μm, so we do not discuss this object further.

REFERENCES

Adams, F. C., Lada, C. J., & Shu, F. H. 1987, ApJ, 312, 788
Agnor, C. B., Canup, R. M., & Levison, H. F. 1999, Icarus, 142, 219
Artymowicz, P. 1988, ApJ, 335, L79
Aumann, H. H., & Probst, R. G. 1991, ApJ, 368, 264
Backman, D. E., & Paresce, F. 1993, in Protostars and Planets III, ed. E. H. Levy & J. I. Lunine (Tucson: Univ. Arizona Press), 1253
Beckwith, S. V. W. 1999, in The Origin of Stars and Planetary Systems, ed. C. J. Lada & N. Kylafis (NATO ASI Ser. C, 540; Dordrecht: Kluwer), 579
Beckwith, S. V. W., Sargent, A. I., Chini, R. S., & Guesten, R. 1990, AJ, 99, 924
Briceño, C., Hartmann, L. W., Stauffer, J. R., Gagné, M., Stern, R. A., & Caillault, J. 1997, AJ, 113, 740
Carballo, R., Wesselius, P. R., & Whittet, D. C. B. 1992, A&A, 262, 106
Carpenter, J. M. 2001, AJ, 121, 2851
Chambers, J. E. 2001, Icarus, 152, 205
Chen, C. H., & Jura, M. 2001, ApJ, 560, L171
Clark, F. O. 1996, PLEXUS, Ver. 2.1a (CD-ROM; Hanscom AFB: Phillips Lab., Dir. Geophys., Air Force Material Command)
Cohen, M., Megeath, S. T., Hammersley, P. L., Martín-Luis, F., & Stauffer, J. 2003a, AJ, 125, 2645
Cohen, M., Schwartz, D. E., Chokshi, A., & Walker, R. G. 1987, AJ, 93, 1199
Cohen, M., Walker, R. G., Carter, B., Hammersley, P., Kidger, M., & Noguchi, K. 1999, AJ, 117, 1864
Cohen, M., Wheaton, W. A., & Megeath, S. T. 2003b, AJ, 126, 1090
Cutispoto, G., Pastori, L., Pasquini, L., de Medeiros, J. R., Tagliaferri, G., & Andersen, J. 2002, A&A, 384, 491
Cutri, R. M., et al. 2003, 2MASS All-Sky Catalog of Point Sources (Pasadena: IPAC)
de Bruijne, J. H. J. 1999, MNRAS, 306, 381
Dohnanyi, J. W. 1969, J. Geophys. Res., 74, 2531
Dominik, C., & Decin, G. 2003, ApJ, 598, 626
Dunkin, S. K., Barlow, M. J., & Ryan, S. G. 1997, MNRAS, 290, 165
ESA. 1997, The *Hipparcos* and Tycho Catalogues (ESA SP-1200; Noordwijk: ESA)
Fajardo-Acosta, S. B., Beichman, C. A., & Cutri, R. M. 2000, ApJ, 538, L155
Fixsen, D. J., & Dwek, E. 2002, ApJ, 578, 1009
Gaidos, E. J. 1999, ApJ, 510, L131
Ghez, A. M., Neugebauer, G., & Matthews, K. 1993, AJ, 106, 2005
Golay, M. 1974, Introduction to Astronomical Photometry (Dordrecht: Reidel)
Greenberg, R., & Nolan, M. C. 1989, in Asteroids II, ed. R. P. Binzel, T. Gehrels, & M. S. Matthews (Tucson: Univ. Arizona Press), 778
Grün, E., Zook, H. A., Fechtig, H., & Giese, R. H. 1985, Icarus, 62, 244
Habing, H. J., et al. 2001, A&A, 365, 545
Haisch, K. E., Lada, E. A., & Lada, C. J. 2001a, ApJ, 553, L153
———. 2001b, AJ, 121, 2065
Harper, D. A., Loewenstein, R. F., & Davidson, J. A. 1984, ApJ, 285, 808
Hartmann, W. K., & Davis, D. R. 1975, Icarus, 24, 504
Hawley, S. L., Gizis, J. E., & Reid, I. N. 1996, AJ, 112, 2799
Henize, K. G. 1976, ApJS, 30, 491
Hillenbrand, L. A., Strom, S. E., Calvet, N., Merrill, K. M., Gatley, I., Makidon, R. B., Meyer, M. R., & Skrutskie, M. F. 1998, AJ, 116, 1816
Hinz, P. M., Angel, J. R. P., Woolf, N. J., Hoffmann, W. F., & McCarthy, D. W. 2000, Proc. SPIE, 4006, 349
Hoffmann, W. F., & Hora, J. L. 1999, MIRAC3 User's Manual (Tucson: Steward Obs.)
Hoffmann, W. F., Hora, J. L., Fazio, G. G., Deutsch, L. K., & Dayal, A. 1998, Proc. SPIE, 3354, 647
Høg, E., et al. 2000, A&A, 355, L27
Hora, J. L. 1991, Ph.D. thesis, Univ. Arizona
IPAC. 1986, *IRAS* Point Source Catalog (Pasadena: IPAC)
Jayawardhana, R., Hartmann, L., Fazio, G., Fisher, R. S., Telesco, C. M., & Piña, R. K. 1999, ApJ, 521, L129
Kelsall, T., et al. 1998, ApJ, 508, 44
Kenyon, S. J., & Bromley, B. C. 2004, ApJ, 602, L133
Kenyon, S. J., & Hartmann, L. 1995, ApJS, 101, 117
Kleine, T., Mezger, K., & Münker, C. 2003, Meteoritics Planet. Sci., 38, 5212
Kleine, T., Münker, C., Mezger, K., & Palme, H. 2002, Nature, 418, 952
Kohoutek, L. 2001, A&A, 378, 843
Lagrange, A.-M., Backman, D. E., & Artymowicz, P. 2000, Protostars and Planets IV, ed. V. Mannings, A. Boss, & S. S. Russell (Tucson: Univ. Arizona Press), 639
Lawson, W. A., Crause, L. A., Mamajek, E. E., & Feigelson, E. D. 2002, MNRAS, 329, L29
Lawson, W. A., Lyo, A.-R., & Muzerolle, J. 2004, MNRAS, 351, L39
Lyo, A.-R., Lawson, W. A., Mamajek, E. E., Feigelson, E. D., Sung, E., & Crause, L. A. 2003, MNRAS, 338, 616
Mamajek, E. E., Meyer, M. R., & Liebert, J. 2002, AJ, 124, 1670
Marcy, G. W., & Butler, R. P. 2000, PASP, 112, 137

Mathioudakis, M., & Doyle, J. G. 1993, A&A, 280, 181
Mathis, J. S., Rumpl, W., & Nordsieck, K. H. 1977, ApJ, 217, 425
McCaughrean, M. J., & O'Dell, C. R. 1996, AJ, 111, 1977
Metchev, S. A., Hillenbrand, L. A., & Meyer, M. R. 2004, ApJ, 600, 435
Meyer, M. R., et al. 2002, The Origins of Stars and Planets: The VLT View, ed. J. F. Alves & M. J. McCaughrean (Berlin: Springer), 463
———. 2004, ApJS, 154, 422
Moshir, M., et al. 1990, *IRAS* Faint Source Catalog, Ver. 2.0 (Pasadena: IPAC)
Muzerolle, J., Calvet, N., Briceño, C., Hartmann, L., & Hillenbrand, L. 2000, ApJ, 535, L47
Muzerolle, J., Calvet, N., Hartmann, L., & D'Alessio, P. 2003, ApJ, 597, L149
Nelson, G. J., Robinson, R. D., Slee, O. B., Ashley, M. C. B., Hyland, A. R., Tuohy, I. R., Nikoloff, I., & Vaughan, A. E. 1986, MNRAS, 220, 91
Pottasch, S. R., & Parthasarathy, M. 1988, A&A, 192, 182
Preibisch, T., Guenther, E., Zinnecker, H., Sterzik, M., Frink, S., & Roeser, S. 1998, A&A, 333, 619
Preibisch, T., & Zinnecker, H. 1999, AJ, 117, 2381
Probst, R. G. 1983, ApJS, 53, 335
Randich, S., Pallavicini, R., Meola, G., Stauffer, J. R., & Balachandran, S. C. 2001, A&A, 372, 862
Reid, I. N., Kilkenny, D., & Cruz, K. L. 2002, AJ, 123, 2822
Siess, L., Dufour, E., & Forestini, M. 2000, A&A, 358, 593
Siess, L., Forestini, M., & Dougados, C. 1997, A&A, 324, 556
Silverstone, M. D. 2000, Ph.D. thesis, UCLA
Skrutskie, M. F., Dutkevitch, D., Strom, S. E., Edwards, S., Strom, K. M., & Shure, M. A. 1990, AJ, 99, 1187
Soderblom, D. R., Jones, B. F., Balachandran, S., Stauffer, J. R., Duncan, D. K., Fedele, S. B., & Hudon, J. D. 1993, AJ, 106, 1059
Song, I., Weinberger, A. J., Becklin, E. E., Zuckerman, B., & Chen, C. 2002, AJ, 124, 514
Spangler, C., Sargent, A. I., Silverstone, M. D., Becklin, E. E., & Zuckerman, B. 2001, ApJ, 555, 932
Stapelbroek, M. G., Seib, D. H., Huffman, J. E., & Florence, R. A. 1995, Proc. SPIE, 2475, 41
Stelzer, B., & Neuhäuser, R. 2001, A&A, 372, 117
Stevenson, D. J. 1987, Annu. Rev. Earth Planet. Sci., 15, 271
Sylvester, R. J., Skinner, C. J., Barlow, M. J., & Mannings, V. 1996, MNRAS, 279, 915
Torres, C. A. O., da Quast, G. R., de la Reza, R., da Silva, L., & Melo, C. H. F. 2001, in ASP Conf. Ser. 244, Young Stars Near Earth, ed. R. Jayawardhana & T. P. Greene (San Francisco: ASP), 43
Torres, C. A. O., da Silva, L., Quast, G. R., de la Reza, R., & Jilinski, E. 2000, AJ, 120, 1410 (TDQ00)
van der Bliek, N. S., Manfroid, J., & Bouchet, P. 1996, A&AS, 119, 547
Waters, L. B. F. M., Cote, J., & Aumann, H. H. 1987, A&A, 172, 225
Weidenschilling, S. J. 1977, Ap&SS, 51, 153
Weinberger, A. J., Becklin, E. E., Zuckerman, B., & Song, I. 2003a, BAAS, 202, 34.01
———. 2003b, BAAS, 203, 13.03
Wetherill, G. W., & Stewart, G. R. 1993, Icarus, 106, 190
Whittet, D. C. B. 2003, Dust in the Galactic Environment (2nd ed.; Bristol: IOP)
Wichmann, R., Schmitt, J. H. M. M., & Hubrig, S. 2003, A&A, 399, 983
Wolf, S., & Hillenbrand, L. A. 2003, ApJ, 596, 603
Wolfe, W. L., & Zissis, G. J. 1985, The Infrared Handbook (Arlington: Office of Naval Research)
Wolk, S. J., & Walter, F. M. 1996, AJ, 111, 2066
Zacharias, N., Urban, S. E., Zacharias, M. I., Wycoff, G. L., Hall, D. M., Monet, D. G., & Rafferty, T. J. 2004, AJ, 127, 3043
Zuckerman, B., & Song, I. 2004, ApJ, 603, 738
Zuckerman, B., Song, I., Bessell, M. S., & Webb, R. A. 2001a, ApJ, 562, L87
Zuckerman, B., Song, I., & Webb, R. A. 2001b, ApJ, 559, 388 (ZSW01)
Zuckerman, B., & Webb, R. A. 2000, ApJ, 535, 959 (ZW00)